RSC Advances

PAPER

View Article Online
View Journal | View Issue

Cite this: *RSC Adv.*, 2017, **7**, 50127

The catalytic performances and reaction mechanism of nanoparticle Cd/Ce–Ti oxide catalysts for NH_3-SCR reaction†

Zhichen Duan,[a] Kebin Chi,[b] Jian Liu,*[a] Juan Shi,[a] Zhen Zhao,[a] Yuechang Wei[a] and Weiyu Song[a]

$Ce_{0.3}$–TiO_x nanoparticle carrier was prepared by the sol–gel method, and a series of Cd–Ce–Ti nanoparticle catalysts with variable Cd contents were prepared by the means of an improved incipient-wetness impregnation. The catalysts were characterized by means of XRD, N_2 adsorption–desorption analysis, SEM, TEM, NH_3-TPD and *in situ* DRIFTS. The catalytic activities for deNO_x were evaluated by NH_3-SCR reaction. All these nanoparticle catalysts contain mesopores with a pore size around 7 nm, and the average particle size is 20 nm. Among the catalysts, 2 wt% Cd/$Ce_{0.3}TiO_x$ catalyst exhibits the best NH_3-SCR performance with a wide temperature window of 250–400 °C for NO conversion above 90%. Moreover, *in situ* DRIFTS spectra of NO_x reduction over 2 wt% Cd/$Ce_{0.3}TiO_x$ catalyst were also investigated. The results show that this reaction mainly follows the Langmuir–Hinshelwood mechanism at room temperature, while Eley–Rideal mechanism plays more important role when the reaction temperature is higher than 150 °C. The adsorbed NH_3 coordinately linked to Lewis acid site is easy to react with NO_x at high temperature.

Received 21st June 2017
Accepted 18th October 2017

DOI: 10.1039/c7ra06931f

rsc.li/rsc-advances

1. Introduction

It is generally considered that the air pollution is predominantly from combustion processes of fossil fuels in power plants, vehicles and other incineration processes. Among various air contaminants, nitrogen oxides (NO_x) are notable and known as major causes of photochemical smog, haze, acid rain, ozone depletion and the greenhouse effect.[1,2] Selective catalytic reduction of NO_x with NH_3 (NH_3-SCR) is a powerful technique for the abatement of NO_x from stationary sources. WO_3 (MoO_3) modified V_2O_5/TiO_2 are the current commercially used catalysts for NH_3-SCR in industry.[3–5] However, some disadvantages still exist in these catalyst systems, including high working temperature, toxicity of vanadium species and low N_2 selectivity at high temperatures.[6,7] Therefore, many researchers are trying to develop new NH_3-SCR catalysts with high deNO_x efficiency, high N_2 selectivity, excellent hydrothermal stability and insensitivity to co-existing poisoning components in SCR atmosphere such as H_2O, SO_2 or alkali metals *etc.*[8–10]

In recent years, Ce–Ti based catalysts for NH_3-SCR reaction have been attracted much attention from researchers. This kind of catalyst indeed offers a number of advantages over V–Ti catalysts. They are active and selective in a wider temperature range, nontoxic, and high N_2 selectivity even at high temperatures.[11–14] The transition metal Cd, is belong to IIB elements, and has attracted attention in environmental catalysis, photocatalysis and hydrodesulfurization.[15,16] However, there is lack to study for NO_x reduction. By the incorporation of metal oxide Cd into the ceria lattice, it is beneficial to the formation of mixed oxides or solid solutions.

In this work, $Cd_M/Ce_{0.3}$–TiO_x nanoparticle catalysts were prepared by the incipient-wetness impregnation method with different Cd contents for improving the catalytic performances for the SCR of NO with NH_3. Their physicochemical properties were investigated systematically.

2. Experimental

2.1 Catalyst preparation

$Ce_{0.3}$–TiO_2 nanoparticle carrier was prepared by the sol–gel method. All chemicals were of analytical grade. A solution of deionized water (2 ml), anhydrous ethanol (10 ml) and a certain amount of cerium nitrate were vigorously stirred at room temperature. The solution was added dropwise into the mixing solution of butyl titanate (10 g) and anhydrous ethanol (30 ml), and then a certain amount of hydrochloricacid was added to adjust pH until pH = 1. The obtained mixture was stirred for 4 h

[a]*State Key Laboratory of Heavy Oil Processing, Beijing Key Lab of Oil & Gas Pollution Control, China University of Petroleum, 18# Fuxue Road, Chang Ping District, Beijing 102249, China. E-mail: liujian@cup.edu.cn; Fax: +86-10-69724721; Tel: +86-10-89732278*

[b]*Petrochemical Research Institute, Petro China Company Limited, Beijing 100195, China*

† Electronic supplementary information (ESI) available. See DOI: 10.1039/c7ra06931f

and placed at room temperature for about 2 days to form a gelatum. Then the gelatum was dried at 100 °C for 24 h and calcined at 500 °C for 4 h in air. The sample is denoted as $Ce_{0.3}TiO_x$, where the molar ratio of Ce and Ti is 0.3 : 1.

A series of $Cd_M/Ce_{0.3}TiO_x$ (M = 1, 2, 3, 5, wt%) nanoparticle catalysts with fixed Ce/Ti molar ratio of 0.3 and fixed Cd loading amounts of M% were prepared by an improved incipient-wetness impregnation method. In a typical synthesis, the support of 5 g $Ce_{0.3}TiO_x$ was preheated in a vacuum oven at 100 °C to remove the adsorbed water. Then an aqueous solution of $Cd(CH_3COO)_2$ was slowly added to the support at stirring with a glass rod under room temperature, and then ultrasonic treatment for 1 h. The precursor was dried at 100 °C for 12 h, and consequently calcined in air at 500 °C for 6 h. The final catalyst is labeled as $Cd_M/Ce_{0.3}TiO_x$ (M = 1, 2, 3, 5, wt%).

2.2 Catalyst characterization

Powder XRD patterns were obtained by a powder X-ray diffractometer (Shimadzu XRD 6000) using Cu Kα (λ = 0.15406 nm) radiation with a Nickel filter and operating at 40 kV and 10 mA in the 2θ range of 5–70° at a scanning rate of 1°min^{-1}.

N_2 adsorption–desorption isotherm was measured at 77 K using a Micromeritics TriStar II 2020 porosimetry analyzer. The samples were degassed at 300 °C for 8 h prior to the measurements. The specific surface areas were calculated according to the Brunauer–Emmett–Teller (BET) method.

The surface morphology of the catalyst was observed by field emission scanning electron microscopy (FESEM) on a Quanta 200F instrument using accelerating voltages of 5 kV, in combination with an EDAX genesis 4000 energy-dispersive X-ray spectrometer (EDX). TEM images were carried out using a JEOL JEM 2100 electron microscope equipped with a field emission source at an accelerating voltage of 200 kV.

Temperature-programmed desorption of ammonia (NH_3-TPD) measurement was performed on a conventional flow apparatus. Prior to measurements, 100 mg of the sample was pretreated in N_2 gas (60 cm^3 min^{-1}) at 500 °C for 0.5 h and then cooled down to room temperature. Next, the sample was exposed to a mixed gas (10 vol% NH_3 and 90 vol% N_2) flow of 30 cm^3 min^{-1} for 0.5 h to ensure the sufficient adsorption of NH_3. Before desorption, the sample was flushed in N_2 gas for 1.5 h. Subsequently, NH_3 desorption was performed in the range of 50–600 °C at a heating rate of 10 °C min^{-1} under a N_2 flow of 30 cm^3 min^{-1}.

In situ DRIFTS were recorded using a thermo Nicolet IS50 spectrometer, which was equipped with a high temperature environmental cell fitted with Zn–Se window and an MCT detector cooled with liquid N_2. The catalyst was loaded in the Harrick IR cell and heated to 400 °C under N_2 at a total flow rate of 50 cm^3 min^{-1} for 60 min to remove adsorbed impurities. A background spectrum was collected under a flowing N_2 atmosphere and was subtracted from the sample spectra. The *in situ* DRIFTS spectra were recorded by accumulating 64 scans with a resolution of 4 cm^{-1}.

2.3 Catalytic activity measurement

NH_3-SCR activity measurements were carried out in a fixed bed quartz micro-reactor operating in a steady flow mode. 0.4 g of catalysts were sieved with 40–60 mesh and used in each test. The reactant gas included 1000 ppm NO, 1000 ppm NH_3, 3% O_2 and balance N_2. The total flow rate was 500 cm^3 min^{-1} and thus a GHSV of 45 000 h^{-1} was obtained. The temperature varied from 100 to 500 °C, and heating rate was 3 °C min^{-1}. The data was recorded when the temperature hold at each point for more than 5 min. The concentration of NO_x (NO_x = NO + NO_2) in the inlet and outlet gas mixture was measured by a SIGNAL 4000 VM NO_x analyzer. Meanwhile, the concentration of NH_3, NO, NO_2 and N_2O were measured by a FTIR spectrometer (MKS, Multi Gas 2030HS).

NO conversion and N_2 selectivity are calculated in the following eqn (1) and (2).

$$\text{NO conversion} = \frac{[\text{NO}]_{\text{inlet}} - [\text{NO}]_{\text{outlet}}}{[\text{NO}]_{\text{inlet}}} \times 100\% \quad (1)$$

$$N_2 \text{ selectivity} = \left(1 - \frac{2[N_2O]_{\text{outlet}}}{[NO_x]_{\text{inlet}} + [NH_3]_{\text{inlet}} - [NO_x]_{\text{outlet}} - [NH_3]_{\text{outlet}}}\right) \times 100\% \quad (2)$$

3. Results and discussion

3.1 XRD results

XRD was employed to analyze the phase structure of all the catalysts. Fig. 1 shows the XRD patterns of $Cd_M/Ce_{0.3}$–TiO_x mixed-oxide catalysts. Crystalline phases were identified by comparison with ICDD files (anatase TiO_2, 21-1272; CeO_2, 34-0394). Among them, titanium oxide was a dominating phase. As shown in Fig. 1, the diffraction peaks at 25.58°, 28.62°, 47.61°, 56.47°, are ascribed to the characteristic reflections of anatase TiO_2. There is no peak at 27.5° in the samples, which indicates that there is no rutile titania existing in all samples.[17,18] Moreover, there is a characteristic peak assigned to Cd oxide (peak at 33.24°).[19] This indicates that Cd oxides are dispersed over $Ce_{0.3}TiO_x$ support for $Cd_M/Ce_{0.3}$–TiO_x samples.

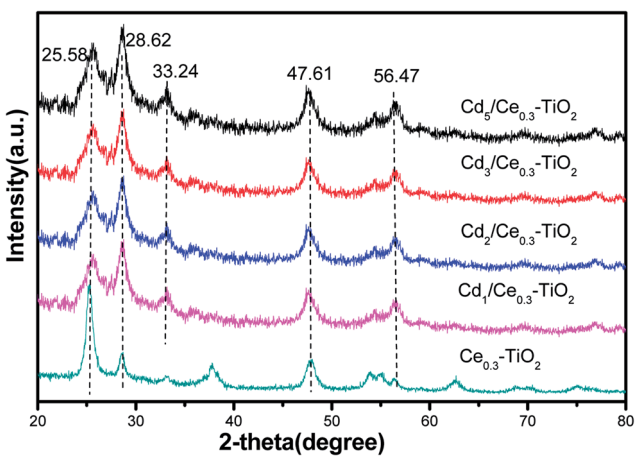

Fig. 1 XRD patterns of the $Cd_M/Ce_{0.3}$–TiO_x catalysts.

Table 1 BET surface areas and structural parameters of $Cd_M/Ce_{0.3}$–TiO_x catalysts

Sample	S_{BET}[a] ($m^2\ g^{-1}$)	d_p[b] (nm)	V_p[b] ($cm^3\ g^{-1}$)
$Ce_{0.3}$–TiO_x	45.8	7.9	0.15
$Cd_1/Ce_{0.3}$–TiO_x	69.0	7.4	0.18
$Cd_2/Ce_{0.3}$–TiO_x	67.1	7.3	0.18
$Cd_3/Ce_{0.3}$–TiO_x	57.7	7.4	0.16
$Cd_5/Ce_{0.3}$–TiO_x	56.9	7.5	0.17

[a] Calculated by BET method. [b] Calculated by *t*-plot method.

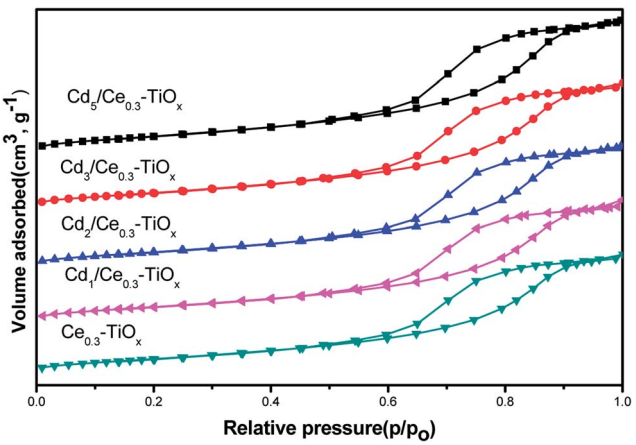

Fig. 2 Nitrogen adsorption–desorption isotherms of the $Cd_M/Ce_{0.3}$–TiO_x catalysts.

3.2 N_2 adsorption–desorption results

BET surface areas and structural parameters of $Cd_M/Ce_{0.3}$–TiO_x catalysts were measured by N_2 adsorption–desorption. Table 1 summarizes the surface area (S_{BET}), pore volume (V_p), and pore diameter (d_p) of different samples, calculated by the BJH method based on the N_2 adsorption–desorption isotherms. It is clear that $Ce_{0.3}$–TiO_x exhibits the lowest S_{BET} values about 45.8 $m^2\ g^{-1}$, while all $Cd_M/Ce_{0.3}$–TiO_x exhibit the higher S_{BET} values about 56.9–69.0 $m^2\ g^{-1}$. It may be due to an interaction between $Ce_{0.3}$–TiO_x and CH_3COO^- ions. In the process of impregnation, $Cd(CH_3COO)_2$ was used. The pore wall of the support $Ce_{0.3}$–TiO_x was acid corrosion by CH_3COO^- ions and the pore volume of the catalysts was enlarged. Thus, $Cd_M/Ce_{0.3}$–TiO_x exhibits the higher S_{BET} values. BET surface area decreases when Cd contents increase. It may be due to excess Cd blocking the pores of the catalysts with the increasing of Cd contents. N_2 adsorption–desorption result also shows that all samples contain mesopores with a relatively uniform pore size around 7 nm. Meanwhile, the isotherm curves of $Cd_M/Ce_{0.3}$–TiO_x catalysts show typical H1 hysteresis loop (Fig. 2). It indicates the mesoporous structure of the mixed oxide.[20] The pore size distribution is concentrated. There is no additional pore-forming material was used in the process of catalyst preparation. Thus, the mesoporous structure may be produced by the aggregation of nanoparticles.

3.3 SEM results

The microstructure of all catalysts was further investigated by SEM. In Fig. 3a, $Ce_{0.3}$–TiO_x sample is composed of irregularly localized and distinct edged particles within the regular geometry (nanoparticles). The images in Fig. 3b–e show the agglomeration degree of catalysts varies with different Cd loading amounts. There is no obvious effect on the catalyst morphology when Cd content is low. However, when the loading amount is more than 3 wt%, the catalyst surface agglomeration becomes slightly clear.

3.4 TEM results

TEM image of $Cd_2/Ce_{0.3}$–TiO_x nanoparticle catalyst is shown in Fig. 4. The lattice fringe, which is marked as 0.35 nm in the HRTEM image of $Cd_2/Ce_{0.3}$–TiO_x, belongs to (101) planes of anatase TiO_2.[20,21] The lattice fringe, which is marked as 0.32 nm in the HRTEM image of $Ce_{0.3}$–TiO_2, belongs to (111) planes of CeO_2. $Cd_M/Ce_{0.3}$–TiO_x nanocomposites show a uniform distribution and small particle sizes. The mean diameters were analyzed by statistical analysis of more than 100 particles in TEM images. The average particle size is 20 nm for $Cd_M/Ce_{0.3}$–TiO_x catalysts. The sample displays a uniform distribution of particle sizes.

3.5 NH_3-TPD results

Temperature-programmed desorption of ammonia was carried out to determine the strength and amount of different acid sites. NH_3-TPD patterns of $Cd_M/Ce_{0.3}$–TiO_x catalysts are depicted in Fig. 5. All catalysts show two shoulder peaks in the ranged 140–360 °C and 450–600 °C, respectively. The ammonia desorbed at low temperatures is ascribed to the weak acidic sites, which is corresponding to the partially ionic NH_4^+ bound to Brønsted acid sites. And the ammonia desorbed at high temperature was ascribed to the desorption of co-ordinated NH_3 bound Lewis acid sites.[6,22,23]

Furthermore, the intensity and the area of NH_3 desorption over $Cd_2/Ce_{0.3}$–TiO_x is higher than the other catalyst. The comparison of the area of the desorbed NH_3 over $Ce_{0.3}$–TiO_x, $Cd_2/Ce_{0.3}$–TiO_x and $Cd_5/Ce_{0.3}$–TiO_x catalysts is 1 : 1.06 : 0.87. The ammonia adsorption ability of the catalyst is generally considered as one of the most important criteria for the screening of catalytic systems for the NH_3-SCR.[6,22,23] As was shown in Fig. 5, $Cd_2/Ce_{0.3}$–TiO_x catalyst showed more desorbed ammonia at low temperature. It seems that the proper content of Cd catalyst possesses more weak acidic sites. Thus, the improvement in ammonia adsorption over $Cd_2/Ce_{0.3}$–TiO_x catalyst is believed to be significantly beneficial to the NO_x reduction by ammonia.

3.6 NH_3-SCR activities

Fig. 6 shows the results of NO conversion in NH_3-SCR reaction over $Cd_M/Ce_{0.3}$–TiO_x catalysts in the temperature range of 175–400 °C, and Fig. 7 shows the N_2 selectivity of $Cd_2/Ce_{0.3}$–TiO_x catalysts in the temperature range of 175–400 °C. And a commercial $V_2O_5/WO_3/TiO_2$ catalyst was used as a ref. 6, 24 and 25. When appropriate amounts of Cd are loaded to $Ce_{0.3}$–

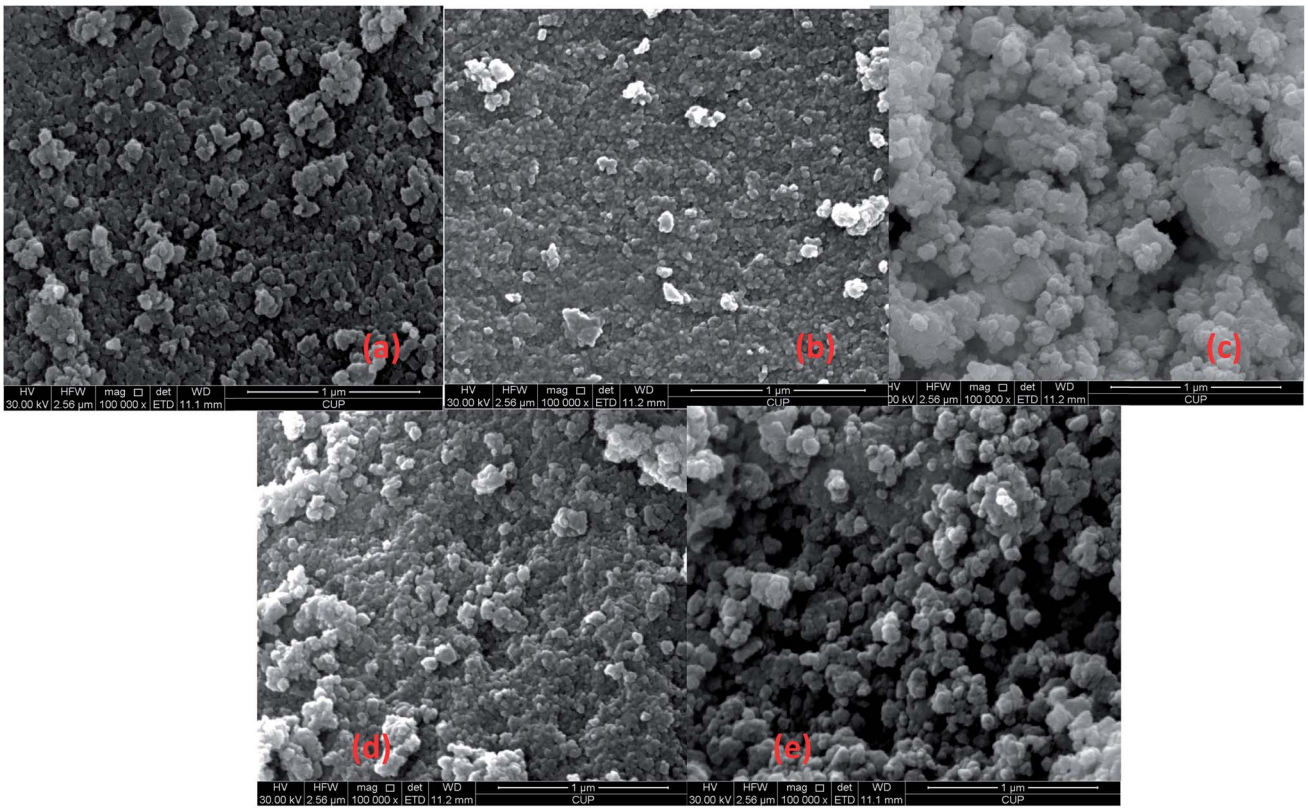

Fig. 3 SEM images of different catalysts: (a) $Ce_{0.3}$–TiO_x, (b) $Cd_1/Ce_{0.3}$–TiO_x (c) $Cd_2/Ce_{0.3}$–TiO_x (d) $Cd_3/Ce_{0.3}$–TiO_x (e) $Cd_5/Ce_{0.3}$–TiO_x.

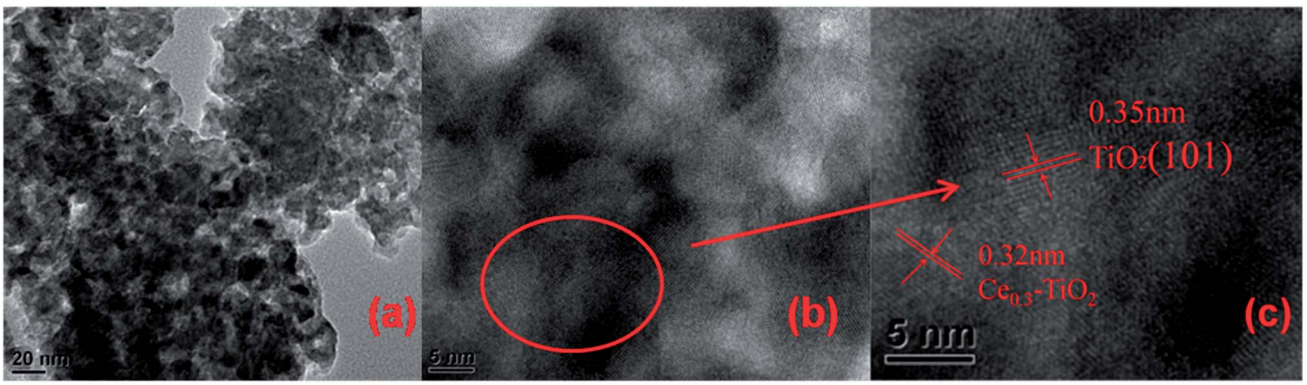

Fig. 4 TEM images of $Cd_2/Ce_{0.3}$–TiO_x catalysts.

TiO_x, a significant influence on catalytic activity is observed. The temperature range for optimum NO reduction (>90%) extends toward wider temperature window. Among all the catalysts tested in this study, $Cd_2/Ce_{0.3}$–TiO_x catalyst exhibits the widest temperature window of catalytic activity for the removal of NO. The highest temperature to maintain NO conversion of 90% is 400 °C. For $Cd_2/Ce_{0.3}$–TiO_x catalyst, the temperature range is between 250 °C and 400 °C for NO removal above 90%. Meanwhile, the large amounts of Cd addition (3 wt% and 5 wt%) lead to a decreasing activity, which may be due to the occurrence of unselective oxidation of NH_3. The catalytic performances of $Cd_1/Ce_{0.3}$–TiO_x catalyst and $Cd_2/Ce_{0.3}$–TiO_x catalyst are very similar in the temperature range between 325 and 400 °C. However, the catalytic behaviours of $Cd_M/Ce_{0.3}$–TiO_x catalysts are associated with the amount of Cd addition in the whole temperature range.

$Cd_2/Ce_{0.3}$–TiO_x exhibits the highest catalytic activity among $Cd_M/Ce_{0.3}$–TiO_x catalysts. In the temperature range of 250–400 °C, NO_x conversion exceeds 90%, which is better than the commercial V–W–Ti catalyst. More remarkably, N_2 selectivity is kept above 96% in the range of 175–400 °C, while the N_2 selectivity of V–W–Ti catalyst is 87% at 400 °C.

Cd belongs to IIB elements and its main valence state is Cd^{2+}. Similar to TiO_2, Cd has also exhibited very high photocatalytic

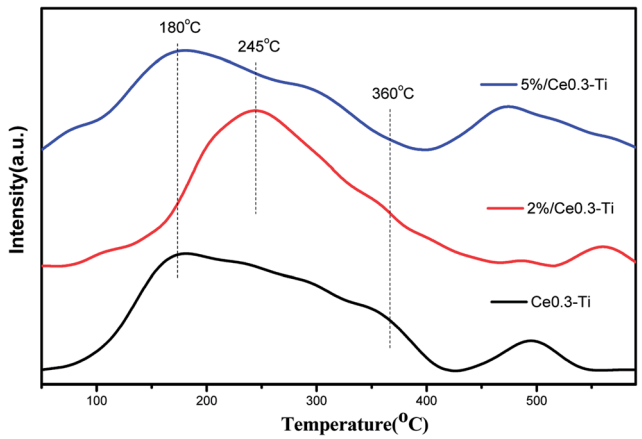

Fig. 5 NH_3-TPD curves of $Ce_{0.3}$–TiO_x, $Cd_2/Ce_{0.3}$–TiO_x and $Cd_5/Ce_{0.3}$–TiO_x catalysts.

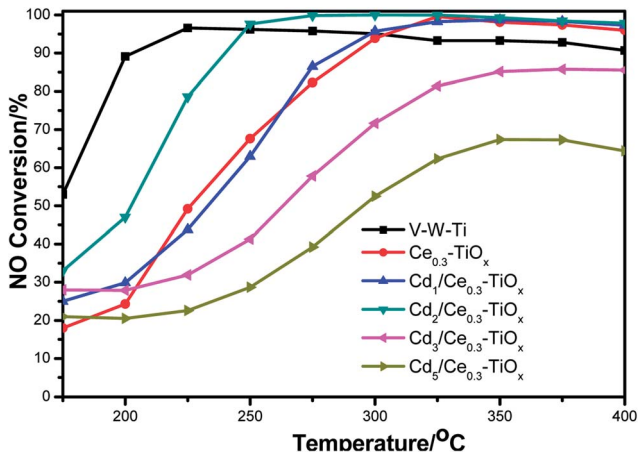

Fig. 6 NO conversion as a function of reaction temperature over $Cd_M/Ce_{0.3}$–TiO_x catalysts.

activity.[15,16] It may indicate that there is the strong interaction a synergistic effect between Cd and TiO_x. And a proper content of Cd promotes the catalytic activity of $Cd_M/Ce_{0.3}$–TiO_x catalyst for

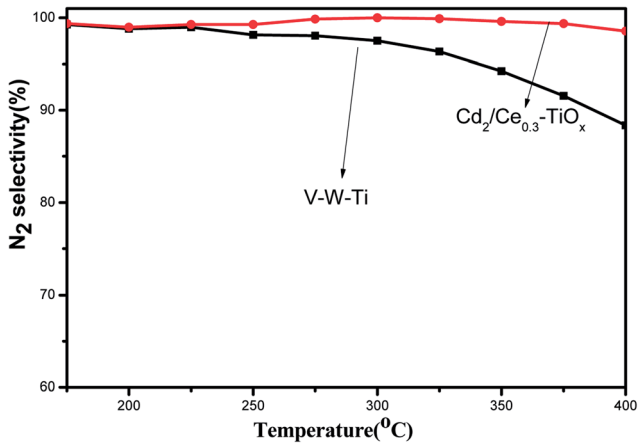

Fig. 7 N_2 selectivity as a function of reaction temperature over $Cd_2/Ce_{0.3}$–TiO_x and V–W–Ti catalysts.

NH_3-SCR reaction. The NO conversion in NH_3-SCR reaction show that 2 wt% $Cd/Ce_{0.3}$–TiO_x is the better than other samples. It may be due to more uniformly catalyst particles, bigger surface area and excellent physicochemical properties.

Furthermore, it should be noted that the NO conversion decreased at 400 °C or higher temperature and the NO conversion decreases with the increasing of the reaction temperature due to the more unselective oxidation of NH_3.

3.7 *In situ* DRIFTS results over $Cd_2/Ce_{0.3}$–TiO_x catalyst

(1) Adsorption of NH_3. The *in situ* DRIFTS of NH_3 adsorption over $Cd_2/Ce_{0.3}$–TiO_x catalyst at different temperatures is shown in Fig. 8. When NH_3 gas is introduced into the DRIFTS cell at room temperature, several vibration bands can be detected in the range of 1000–4000 cm^{-1}. The bands at 1163 and 1207 cm^{-1} can be assigned to the asymmetric and symmetric bending vibrations of N–H bond in NH_3 coordinately linked to Lewis acid site, respectively. The bands at 3354, 3258 and 3153 cm^{-1} can be ascribed to the N–H stretching vibration modes of the coordinated NH_3, while the band at 1435 cm^{-1} with a shoulder at 1472 cm^{-1} is ascribed to the asymmetric bending vibration of NH bond in NH_4^+ chemisorbed on Brønsted acid site.[26,27] These Lewis acid sites on the surface of $Cd_2/Ce_{0.3}$–TiO_x catalyst decrease slowly with the increasing of the reaction temperature. However, it is noticeable that the bands at 1435 and 1472 cm^{-1} are disappeared above 150 °C. It means that those Brønsted acid sites are weak acid sites. The obtained results suggested that at a temperature lower than 200 °C these adsorbed NH_3 species are stable. With the increasing of the temperature, NH_3 is easy to desorb from the weak Brønsted acid sites on the surface of $Cd_2/Ce_{0.3}$–TiO_x catalyst. However, it is stable adsorption on the Lewis acid sites. It has been reported that Brønsted acid site is beneficial for the adsorption of NH_3, thus improving the low-temperature activity.

(2) Co-adsorption of NO and O_2. Fig. 9 shows the *in situ* DRIFTS spectra of NO + O_2 desorption on $Cd_2/Ce_{0.3}$–TiO_x catalyst at different temperatures. Several distinct bands appeared at

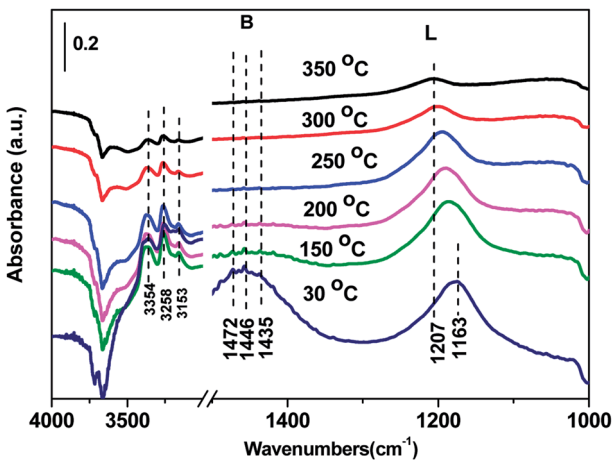

Fig. 8 *In situ* DRIFTS of $Cd_2/Ce_{0.3}$–TiO_x treated in flowing 500 ppm NH_3 at room temperature for 60 min and then purged by N_2 at 30, 150, 200, 250, 300, 350 °C.

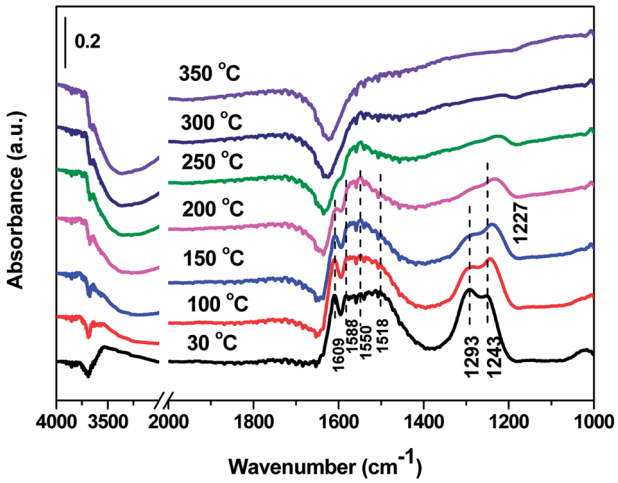

Fig. 9 *In situ* DRIFTS of $Cd_2/Ce_{0.3}$–TiO_x treated in flowing 500 ppm NO + 3% O_2 at room temperature for 60 min and then purged by N_2 at 30, 100, 150, 200, 250, 300, 350 °C.

1243, 1293, 1518, 1588 and 1609 cm^{-1} at room temperature, which was respectively assigned to the asymmetric frequency of gaseous NO_2 molecules (1609 cm^{-1}), bidentate nitrate (1588 cm^{-1}), monodentate nitrate (1293 and 1518 cm^{-1}), bridged nitrate (1243 cm^{-1}). At the temperature 100 °C, the bands ascribed to monodentate nitrate vanished, while the peaks attributed bridged bidentate nitrite (1227 cm^{-1}) and chelating bidentate nitrate (1550 cm^{-1}) appeared, suggesting a redox conversion from monodentate nitrate and bidentate nitrate to *cis*-$N_2O_2^{2-}$, bridged bidentate nitrite and monodentate nitrite over $Cd_2/Ce_{0.3}$–TiO_x catalyst.[28–30] With the increasing of the temperature, all bands attributed to NO_x species vanish gradually, indicating that the absorbed nitrate and nitrite species were decomposed or inhibited.

(3) Reaction between nitrogen oxides and ammonia adspecies. Fig. 10 shows the *in situ* DRIFTS spectra of $Cd_2/Ce_{0.3}$–TiO_x catalyst as a function of time in a flow of NO + 3% O_2 after the catalysts is pre-exposed to a flow of NH_3 for the 60 min followed by N_2 purging for 30 min at 250 °C. The coordinated NH_3 on Lewis acid sites (1210 and 1599 cm^{-1}) and Brønsted acid site (1658 cm^{-1}) were formed after feeding NH_3. The bands at 3386, 3328 and 3196 cm^{-1} can be ascribed to the N–H stretching vibration modes of the coordinated NH_3. All the band due to ammonia adspecies diminish in 10 min after $Cd_2/Ce_{0.3}$–TiO_x catalyst is purged by NO + O_2, and subsequently the absorbed NO_2 (1253 and 1557 cm^{-1}) is observed. It was noticeable that the bands assigned to NO_x species (1606 and 1579 cm^{-1}) are absent and only two bands related to NO_2 appear, indicating that the adsorption of nitrate species is inhibited.[26–32]

(4) Reaction between ammonia and adsorbed nitrogen oxides species. Fig. 11 shows the *in situ* DRIFTS spectra of $Cd_2/Ce_{0.3}$–TiO_x catalyst as a function of time in a flow of NH_3 after the catalyst is pre-exposed to a flow of NO + 3% O_2 for the 60 min followed by N_2 purging for 30 min at 250 °C. The band for the absorbed NO_2 (1610 cm^{-1}) vanished in 5 min after NH_3 were introduced into the system. Simultaneously, the peaks ascribed to coordinated NH_3 on Lewis acid sites (3373, 3259, 3162, 1599 and 1205 cm^{-1}) and NH_4^+ species on Brønsted acid sites (1429 and 1662 cm^{-1}) appear.

(5) *In situ* DRIFTS spectra in a flow of NO + NH_3 + O_2. Fig. 12 shows the *in situ* DRIFTS spectra of $Cd_2/Ce_{0.3}$–TiO_x catalyst in a flowing of 1000 ppm NH_3 + 1000 ppm NO + 3% O_2 at various temperatures under the steady-state condition. NO band assigned to NO_x species is detected in the whole region, which results in the competitive adsorption and follows the reactions among NH_3. With the temperature increasing, the intensity of the bands assigned to NH_4^+ species on Brønsted acid sites (1442, 1674 cm^{-1}) decrease faster than that of the bands ascribed to coordinated NH_3 on Lewis acid sites (3363, 3264, 3168 and 1596 cm^{-1}).[26–32] The adsorbed NH_3 species on Brønsted acid site disappeared completely at 200 °C, while the band at 1203 cm^{-1} attributed to the symmetric bending vibrations of N–H bond in NH_3 coordinately linked to Lewis acid site is also detected even at 350 °C.

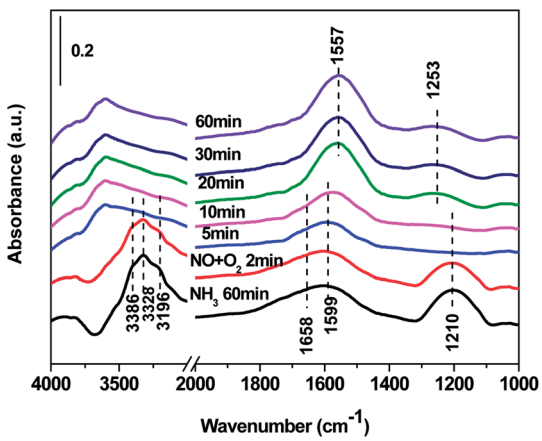

Fig. 10 *In situ* DRIFTS over $Cd_2/Ce_{0.3}$–TiO_x catalyst as a function of time in a flow of NO + 3% O_2 after the catalysts was pre-exposed to a flow of NH_3 for the 60 min followed by N_2 purging for 30 min at 250 °C.

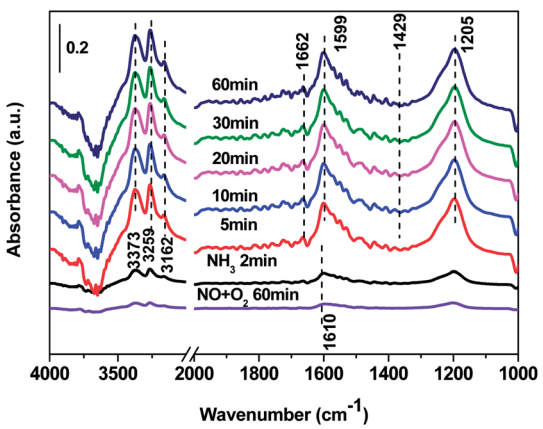

Fig. 11 *In situ* DRIFTS over $Cd_2/Ce_{0.3}$–TiO_x catalyst as a function of time in a flow of NH_3 after the catalysts was pre-exposed to a flow of NO + 3% O_2 for the 60 min followed by N_2 purging for 30 min at 250 °C.

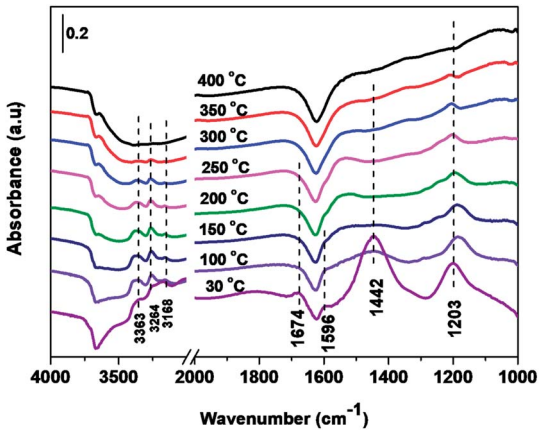

Fig. 12 *In situ* DRIFTS spectra of $Cd_2/Ce_{0.3}$–TiO_x catalyst in a flowing of 1000 ppm NH_3 + 1000 ppm NO + 3% O_2 at 30, 100, 150, 200, 250, 300, 350 and 400 °C.

In situ DRIFTS spectra over $Cd_2/Ce_{0.3}$–TiO_x catalyst show that there is the adsorbed NH_3 species on both Lewis and Brønsted acid site, and the absorbed nitrate and nitrite species form on the surface of catalyst at room temperature. While when the temperature exceeds 150 °C, all bands attributed to NO_x and NH_3 species vanish gradually except the bands attributed to adsorbed NH_3 species on Lewis acid site.

(6) L–H mechanism and E–R-oriented mechanism. The *in situ* DRIFTS spectra indicate that the reaction between absorbed NO_2 and NH_3 easily occurred over $Cd_2/Ce_{0.3}$–TiO_x catalyst. Combining with the result of NO + 3% O_2 adsorption *in situ* DRIFTS, the adsorption of nitrate species is significantly limited, leading to more active sites available for the adsorption and activation of NH_3 thus exhibiting a higher activity. *In situ* DRIFTS spectra in a flow of NO + NH_3 + O_2 exhibits that all the adsorbed NH_3 species on Lewis acid site is detected even at 350 °C. However, NH_3 is easy to desorb from the weak Brønsted acid site at 200 °C. Thus, this phenomenon may be due to the adsorbed NH_3 species on Lewis acid site are very stable and react with NO_2 or NO from the gas phase at 350 °C.

On the one hand, ammonia and nitrogen oxides were adsorbed in low temperature, NH bond in NH_4^+ chemisorbed on acid sites and the bands attributed to NO_x species are obvious. The reaction between adsorbed NO_x and adsorbed ammonia is related to the L–H mechanism. On the other hand, the absorbed nitrate and nitrite species were decomposed at the high temperature, and the absorbed ammonia decreased slowly. The reaction between adsorbed ammonia and NO_2 or NO from the gas phase is corresponding to E–R-oriented mechanism. Thus the *in situ* DRIFTS spectra of $Cd_2/Ce_{0.3}$–TiO_x catalyst show that, the main L–H mechanism may gradually transform to E–R-oriented mechanism with the increasing of the temperature.[26–32]

4. Conclusion

$Ce_{0.3}$–TiO_x nanoparticle carrier was prepared by the sol–gel method, and a series of Cd–Ce–Ti nanoparticle catalysts with variable Cd contents were prepared by the means of an improved incipient-wetness impregnation. The loading amount of Cd in the catalysts affects the NH_3-SCR catalytic activity and physicochemical properties. SEM, TEM and N_2 adsorption–desorption results show that the catalyst particle distributes uniformly and all catalysts contain the mesoporous structure from overlapped nanoparticles.

The NH_3-TPD results indicate that the intensity and the area of NH_3 desorption over $Cd_2/Ce_{0.3}$–TiO_x is higher than the other catalyst. The improvement in ammonia adsorption over $Cd_2/Ce_{0.3}$–TiO_x catalyst is beneficial to the NO_x reduction by ammonia. Among all the catalysts, $Cd_2/Ce_{0.3}$–TiO_x catalyst exhibits the widest temperature window for the removal of NO and the temperature range is between 250 and 400 °C for NO removal above 95%, and the N_2 selectivity is kept above 96% in the full temperature range.

In situ DRIFTS spectra over $Cd_2/Ce_{0.3}$–TiO_x catalyst show that when the temperature exceeds 150 °C, the adsorbed NH_3 species on Lewis acid sites play more important role than those on Brønsted acid sites. With the increasing of the temperature, the main L–H mechanism may gradually transform to E–R-oriented mechanism.

Conflicts of interest

There are no conflicts to declare.

Acknowledgements

This work was financially supported by the National Natural Science Foundation of China (21673290, u1162103 and 21376261), the National Hi-Tech Research and Development Program (863) of China (2015AA034603), and the China Offshore Oil Fund (LHYJYKJSA2016002).

References

1 M. G. Schultz, T. Diehl, G. P. Brasseur and W. Zittel, *Science*, 2003, **302**, 624.
2 Q. Liang, Z. Zhao, J. Liu, Y. Wei, G. Jiangand and A. Duan, *Acta Phys.-Chim. Sin.*, 2014, **30**, 129.
3 A. Tomita, T. Yoshii, S. Teranishi, M. Nagao and T. Hibino, *J. Catal.*, 2007, **247**, 137.
4 X. Zhao, L. Huang, H. Li, H. Hu, J. Han, L. Shi and D. Zhang, *Chin. J. Catal.*, 2015, **36**, 1886.
5 K. Zhao, W. Han, Z. Tang, G. Zhang, J. Lu, G. Lu and X. Zhen, *Colloids Surf., A*, 2016, **503**, 53.
6 K. Cheng, J. Liu, Z. Zhao, Y. Wei, G. Jiang and A. Duan, *RSC Adv.*, 2015, **5**, 45172.
7 H. He, F. Liu, Y. Yu and W. Shan, *Sci. China: Chem.*, 2012, **42**, 442.
8 P. R. Ettireddy, N. Ettireddy, S. Mamedov, P. Boolchand and P. Smimiotis, *Appl. Catal., B*, 2007, **76**, 123.
9 J. Huang, Z. Tong, Y. Huang, Y. Huang and J. Zhang, *Appl. Catal., B*, 2008, **78**, 309.
10 S. Bai, W. Lu, D. Li, X. Li, Y. Fang and L. Yuan, *Acta Phys.-Chim. Sin.*, 2014, **30**, 1107.

11 Z. Liu, S. Zhang and J. Li, *Appl. Catal., B*, 2014, **158**, 11.
12 W. Shan, F. Liu, H. He, C. Deng and X. Zi, *Catal. Commun.*, 2014, **59**, 226.
13 C. Xu, J. Liu, Z. Zhao, F. Yu, K. Cheng, Y. Wei, A. Duan and G. Jiang, *J. Environ. Sci.*, 2015, **31**, 74.
14 R. Wang, L. Lan, M. Gong and Y. Chen, *Acta Phys.-Chim. Sin.*, 2016, **32**, 1747.
15 X. Lu, D. Zheng, J. Gan, Z. Liu, C. Liang, P. Liu and Y. Tong, *J. Mater. Chem.*, 2010, **20**, 9.
16 R. Yang, D. Wang, L. Wan and D. Wang, *RSC Adv.*, 2014, **4**, 22162.
17 W. Wang, S. Wang, X. Ma and J. Gong, *Catal. Today*, 2009, **148**, 323.
18 P. Li, Y. Xin, Q. Li, Z. Wang, Z. Zhang and L. Zheng, *Environ. Sci. Technol.*, 2012, **46**, 9600.
19 G. Zhao, Y. Yang and T. Ren, *Acta Pet. Sin.*, 2006, **22**, 308.
20 G. Leofanti, M. Padovan, G. Tozzola and B. Venturelli, *Catal. Today*, 1998, **41**, 207.
21 H. Wang, S. Cao, F. Zheng, F. Yu, Y. Liu, X. Wei and Z. Wu, *Appl. Surf. Sci.*, 2015, **330**, 245.
22 L. Chen, J. Li, M. Ge and R. Zhu, *Catal. Today*, 2010, **153**(3), 77–83.
23 K. J. Lee, P. A. Kumar, M. S. Maqbool, K. N. Rao, K. H. Song and H. P. Ha, *Appl. Catal., B*, 2013, **142**, 705.
24 A. A. Markeb, L. A. Ordosgoitia, A. Alonso, A. Sánchez and X. Font, *RSC Adv.*, 2016, **6**, 56913.
25 C. Tang, H. Zhang and L. Dong, *Catal. Sci. Technol.*, 2015, **6**, 1248.
26 Z. Liu, S. Zhang, J. Li and L. Ma, *Appl. Catal., B*, 2014, **144**, 90.
27 R. Long and R. Yang, *J. Catal.*, 2000, **190**, 22.
28 G. Ramis, L. Yi and G. Busca, *J. Catal.*, 1995, **157**, 523.
29 F. Liu, H. He, Y. Ding and C. Zhang, *Appl. Catal., B*, 2009, **93**, 194.
30 D. A. Peña, B. S. Uphade and P. G. Smirniotis, *J. Catal.*, 2004, **221**, 421.
31 Y. Li, Y. Li, Y. Wan, S. Zhan, Q. Guan and Y. Tian, *RSC Adv.*, 2016, **6**, 54926.
32 S. Xiong, Y. Liao, H. Dang, F. Qi and S. Yang, *RSC Adv.*, 2015, **5**, 27785.